Third AO4ELT Conference - Adaptive Optics for Extremely Large Telescopes
Florence, Italy. May 2013
ISBN: 978-88-908876-0-4
DOI: 10.12839/AO4ELT3.15023

MULTIPLE OBJECT ADAPTIVE OPTICS: MIXED NGS/LGS TOMOGRAPHY

Tim Morris[1,a], Eric Gendron[2], Alastair Basden[1], Olivier Martin[2], James Osborn[1], David Henry[3], Zoltan Hubert[2], Gaetano Sivo[4,5], Damien Gratadour[2], Fanny Chemla[2], Arnaud Sevin[2], Matthieu Cohen[2], Eddy Younger[1], Fabrice Vidal[2], Richard Wilson[1], Tim Butterley[1], Urban Bitenc[1], Andrew Reeves[1], Nazim Bharmal[1], Henri-Francois Raynaud[4], Caroline Kulcsar[4], Jean-Marc Conan[5], Dani Guzman[6], Javier de Cos Juez[7], Jean-Michel Huet[2], Denis Perret[2], Colin Dickson[3], David Atkinson[3], Tom Baillie[3], Andy Longmore[3], Stephen Todd[3], Gordon Talbot[1], Simon Morris[1], Richard Myers[1] and Gerard Rousset[2]

[1]Durham University, Department of Physics, South Road, Durham, DH1 3LE, UK
[2]Observatoire de Paris, Section de Meudon, 5 Place Jules Janssen, 92195 Meudon Cedex, France
[3]UK Astronomy Technology Centre, Royal Observatory Edinburgh, Blackford Hill, Edinburgh, EH9 3HJ, UK
[4]Laboratoire Charles Fabry, Institut d'Optique Graduate School, CNRS, Université Paris-Sud, Palaiseau, France
[5]Dept. Optique Théorique et Applique, ONERA, Châtillon, France
[6]Dept. of Electrical Engineering, Centre for Astro-Engineering, Pontificia Universidad Catolica de Chile, Vicuña Mackenna 4860, Santiago, Chile
[7]Mining Exploitation and Prospecting Department, C/Independencia n13, University of Oviedo, 33004 Oviedo, Spain

Abstract. Open-loop adaptive optics has been successfully demonstrated on-sky by several groups, including the fully tomographic MOAO demonstration made using CANARY. MOAO instrumentation such as RAVEN will deliver the first astronomical science and other planned instruments aim to extend both open-loop AO performance and the number of corrected fields. Many of these planned systems rely on the use of tomographic open-loop LGS wavefront sensing. Here we present results from the combined NGS/LGS tomographic CANARY system and then compare the NGS- and LGS-based tomographic system performance. We identify the major system performance drivers, and highlight some potential routes for further exploitation of open-loop tomographic AO.

1. Introduction

Multiple Object Adaptive Optics (MOAO) is a control technique that can be used in astronomical AO to compensate for the effects of atmospheric turbulence along several lines of sight distributed within a

a e-mail : t.j.morris@durham.ac.uk

wide (>3 arcminute) field of view. MOAO is targeted at astronomical science cases where there are tens to dozens of objects within a very wide (<10 arcminute) field of view. The fundamental methods that allow MOAO control are tomographic wavefront reconstruction and open-loop control of deformable mirrors.

The combination of these two techniques raises both design and operational issues that can affect system performance. MOAO system performance relies on new and accurate calibration techniques, particularly when Laser Guide Stars (LGS) are used as wavefront references. The presence of both high-order Natural Guide Stars (NGS) and LGS within an open-loop AO system allows for multiple control schemes that can be optimized for a given on-sky target and atmospheric turbulence profile.

In this paper we present an overview of the state of MOAO system development in section 2, in particular concentrating on the CANARY NGS/LGS on-sky demonstrator. In section 3 we describe the Phase B (mixed NGS/LGS MOAO) configuration for CANARY in addition to the instruments used for turbulence profiling. Section 4 presents the initial on-sky and bench results from CANARY Phase B taken during the recent (May 2013) observing run at the 4.2m William Herschel Telescope (WHT).

2. Development of MOAO systems

The key to wide-field adaptive optics correction lies in the 3-dimensional mapping of the full volume of atmospheric turbulence above the telescope. With the knowledge of the vertical distribution of turbulence, usually gained through the monitoring of several guide stars (either natural or laser-based) within a given field of view, the turbulence along a given line of sight, or across a wide-field of view can be calculated.

There have been several multiple guide-star AO systems tested on-sky, such as the multiple LGS-system at the 6.5m Multiple Mirror Telescope (MMT) [2], MAD [3] at the Very Large Telescope, GEMS [4] at Gemini South and the CANARY MOAO demonstrator at the WHT [5]. The multiple-conjugate AO systems, MAD and GEMS use an intentionally-limited form of tomography that restricts wavefront correction to a number of conjugated Deformable Mirrors (DMs) to provide a wide contiguous corrected field of view. Although the tomography in these Multi-Conjugated AO (MCAO) systems is limited, diffraction-limited performance has still been demonstrated [6,7] on-sky over fields of view up to a few arcminutes in diameter enabling exciting new science.

Both CANARY and the MMT do not contain multiple DMs conjugated in altitude, and diffraction-limited performance is limited to narrow fields of view. The tomographic reconstruction from Wavefront Sensor (WFS) data used in these two systems do however allow Ground-Layer AO (GLAO) [8] correction to be determined and applied to the deformable mirror for wide field partial correction. Comparison of performance between GLAO and tomographic AO provides a simple indication of the improvement that can be attained when the vertical distribution of turbulence is known [9,10]. The performance of wavefront tomography is defined not only by the geometry of the NGS/LGS asterism being investigated, but also the turbulence profile.

The other enabling technology required for MOAO operation is open-loop control of the wavefront corrector. On-sky demonstrators such as ViLLaGeS [11] and VOLT [12] proved that the open-loop AO correction is possible, although these were not tomographic systems and investigated only open-loop wavefront control. DMs that are used in open-loop without monitoring by WFSs must either be completely stable and well characterized, or the system must include a separate means for sensing the figure of the DM in real-time to minimize the so-called DM open-loop or go-to error.

The first demonstration of the combination of wavefront tomography with open-loop DM control were undertaken on the laboratory testbenches SESAME and the Tomographic AO testbench at UCSC [13]. These testbenches were used to develop the calibration routines required for MOAO and the experience gained using SESAME was applied to subsequent on-sky experiments such as CANARY.

Several instrument concepts based upon MOAO were developed including FALCON [14] for the 8m VLT and EAGLE [15] for the (then) 42m diameter European ELT. Of these concepts, only the RAVEN instrument [16] has been funded and is planned for installation on the 8m Subaru telescope in 2014. RAVEN contains a 2-channel MOAO system controlled by up to 3 off-axis NGS that can be located within a 3.5 arcminute field of view. RAVEN can also utilize an on-axis sodium LGS system to augment the NGS-only tomography. RAVEN feeds the existing slit based spectrograph mounted on the Subaru Nasmyth platform.

3. CANARY Phase B

CANARY is a dedicated tomographic AO demonstrator that provided the 2010 first demonstration of open-loop correction using tomographic WFS information derived from three off-axis NGS. Unlike the majority of AO systems deployed on large telescopes, CANARY has not been designed to deliver astronomical data, but accurately determine AO system performance. This is primarily achieved using the on-axis reference 'Truth' sensor that observes the open-loop corrected wavefront, with a PSF scoring 'science' camera to measure the system performance in terms of a corrected Strehl ratio.

CANARY is a phased experiment with three planned configurations that take the system from the Phase A NGS-only configuration used in 2010 through to a Phase C configuration that closely matches the proposed architecture for the EAGLE instrument. The Phase B system described here includes a four off-axis LGS WFS in addition to retaining all Phase A (NGS-only) functionality. This brings the total number of *open-loop* high-order wavefront sensors used within the tomographic system to seven. The CANARY instrument control system allows the flexibility to perform tomography using any combination of these reference sources. The NGS slopes can also be processed to provide a tip-tilt only signal.

This allows a wide range of tomographic configurations to be tested using CANARY. 'Full' MOAO using high-order information from all WFSs, open-loop Laser Tomographic AO (LTAO) where only high-order signals from the LGS WFSs are used and tip-tilt is derived from off-axis NGS, and open-loop GLAO can all be investigated through modification of the control matrix uploaded to the real-time control system [17,18]. We can also compare the tomographic performance to closed-loop 'classical' Single-Conjugate AO (SCAO) by controlling the system using the measured wavefront reference from the Truth Sensor.

As at Phase A, CANARY uses a low-order 52-actuator piezo-stack DM controlled in open-loop for wavefront correction. Shack-Hartmann WFS subapertures are 0.6m in diameter when projected onto the WHT pupil. NGS WFS pixel scale is approximately 0.26" per pixel and each subaperture contains 16x16 pixels. The centroiding algorithm uses only the 12 brightest pixels in any given subaperture. The 12 selected pixels are dynamically updated with each frame before centroiding. The LGS WFS pixel scale is approximately 0.47" with each subaperture containing 8x8 pixels. Due to the increased LGS spot size and LGS elongation we use the 20 brightest pixels within each LGS WFS subaperture for wavefront sensing. The system operates at 150Hz due to flux limitations on the NGS, although it can operate at up to 350Hz (limited by maximum camera frame rate). Unless stated otherwise, the LGS are located at a distance of 21km from the telescope pupil. Note that this range gate is fixed and we did not vary the LGS distance with changes in telescope elevation. The LGS altitude is therefore variable and a

function of telescope zenith angle alone. This was taken into account during the determination of the tomographic reconstructor.

Unless stated otherwise, all tomographic control matrices are calculated using the learn and apply method [19]. Once measured, the tomographic reconstructor was used for periods of 30-60minutes before it was recalculated based on changes to the turbulence profile. The closed-loop control matrix is calculated using the MMSE technique.

The other major addition to the real-time control system for Phase B was the implementation of LQG control to allow modal filtering based upon expected atmospheric turbulence statistics. Inclusion of LQG control within the system did improve performance, particularly with respect to telescope vibrations, but also in the presence of high wind speed turbulent layers. Discussion of the LQG control implemented within CANARY is not presented here but additional information and results can be found in the paper of Sivo *et al* [20].

3.1. Photon return

The LGS photon return was measured on-sky in November 2012 by observing a single guide star with a prototype LGS WFS placed behind a KD*P Pockels cell based shutter. The range gate depth was adjusted electronically by varying the shutter open-time and the total observed photon flux measured by the LGS WFS was recorded. Analysis of the LGS WFS spot pattern did not show artefacts associated with ringing such as variations in the illumination along the axis of LGS elongation.

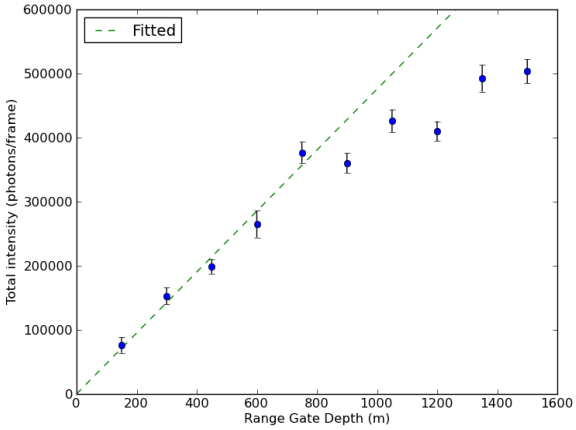

Figure 1 Effect of changing range gate depth on observer photon flux/frame for a single on-axis LGS. Linear fit has been constrained to pass through (0,0) and uses only the first 5 data points.

Figure 1 plots the photon return from a single on-axis 13.5km distant LGS as observed using a 7x7 Shack-Hartmann WFS at an elevation angle of 56 degrees above the horizon. The total output laser power at the laser head was 26.4W at a wavelength of 532nm, although subsequent optics in the launch system meant that the true output power to sky was not measured. The WFS had a 5 arcsecond diameter circular field stop to avoid contamination of adjacent LGS centroids under strong turbulence conditions. The range gate was increased symmetrically around the central 13.5km altitude and for small changes in range gate depth the observed photon flux should increase linearly. The combined effects of varying atmospheric pressure reducing return flux from within the range gate and the LGS spot motion within the field stop causing vignetting can result in a deviation from this linear fit. As such the fit was constrained to return zero photons/frame for a zero depth range gate, and only the first 5 data points (up to a range gate depth of 900m) were used to calculate the base photon return in photons/m of range gate depth/frame.

To create the 4 LGS asterism a Diffractive Optical Element (DOE) is placed into the laser launch system at the entrance to the beam launch telescope. This element splits the incoming single beam into four equal intensity off-axis beams whilst suppressing zeroth-order diffraction. This DOE can then be rotated to match the rotation of the sky. For the single-layer etched transmissive grating used in CANARY we can place 65-67% of the incident light into the first diffracted order to create our LGS asterism. This fraction can be increased using multi-layer etching. LGS asterism spacing is changed by replacing the diffractive element. The plot in Figure 2 shows the number of subapertures across the telescope diameter that could be supported by a 4 LGS asterism that has been created by inserting a DOE into the single LGS launch system. The photon flux limit here has been defined as 200 detected photons/subaperture/frame at the CANARY standard frame rate of 150Hz. This plot shows that for the Phase B system using four 7x7 LGS WFSs the maximum LGS distance that would allow wavefront sensing with an acceptable signal-to-noise ratio is ~23.5km.

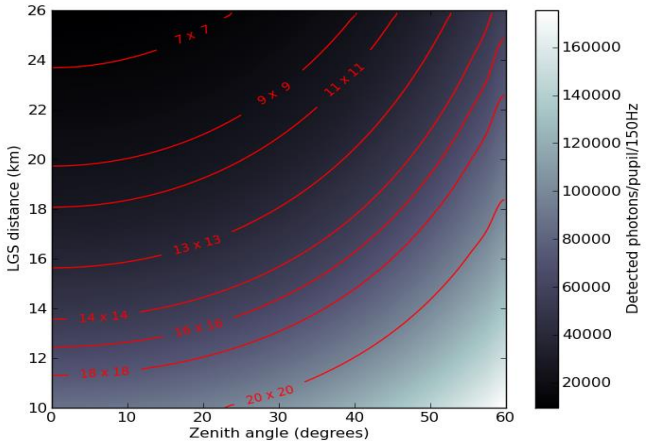

Figure 2 Predicted photon return flux for a 4 LGS asterism when changing LGS distance and telescope zenith angle. Contours plot a photon return of 200 detected photons/subaperture/frame for an NxN subaperture Shack-Hartmann WFS where N ranges from 7 to 20.

3.2. Control of LGS fratricide

CANARY uses a beam launch telescope placed behind the secondary mirror of the WHT. This means that LGS fratricide, where the off-axis laser plume from one LGS contaminates the pupil image for all other WFSs. Rayleigh scattering based LGS systems define the distance between the telescope and wavefront reference through the use of a temporal range gate that is synchronised to the pulsed Rayleigh laser. As such LGS fratricide can be avoided because the LGS WFS is effectively shuttered when the laser pulse is not at the LGS focal distance.

However, the pulsed laser technology used to generate Rayleigh LGS does not operate efficiently below a laser repetition rate of ~10kHz and the output laser power can drop dramatically. This limits the effective maximum altitude that a Rayleigh-based altitude can be used at to below 15km before multiple pulses in flight can cause fratricide effects. Zemax analysis of the optical design of the telescope and LGS WFS however showed that when aligned to an LGS at a focal distance of 20km, the LGS WFS was blind to photon return coming from conjugate altitudes from *any* of the 4 LGS plumes between 9 and 11km (see Figure 3). The LGS WFS was also blind to photon flux below 2km due to secondary shadowing and the LGS field stop.

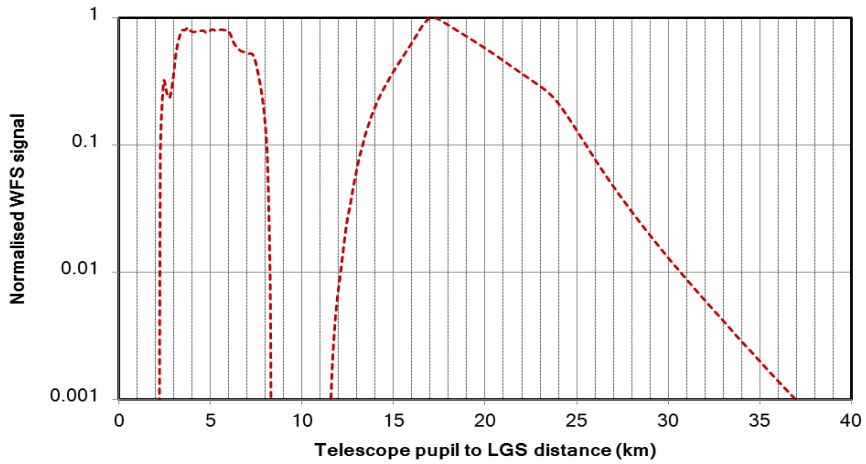

Figure 3 Detected signal from 4 LGS asterism in one Phase B LGS WFS observing an LGS that is 20km distant versus altitude. Signal has been normalized to peak detected signal. Reduction in flux due to increasing LGS altitude with the telescope pointing at zenith has also been modeled.

By tuning the laser pulse frequency, a second pulse can be hidden inside the blocked distance range and the maximum LGS distance can be increased whilst avoiding any fratricide effects. Increasing the LGS WFS focal altitude, or changing the LGS asterism diameter can affect the range of altitudes that cannot be observed by the LGS WFS. The effect of increasing the laser pulse rate from 10kHz to 12kHz on LGS fratricide is shown in Figure 4.

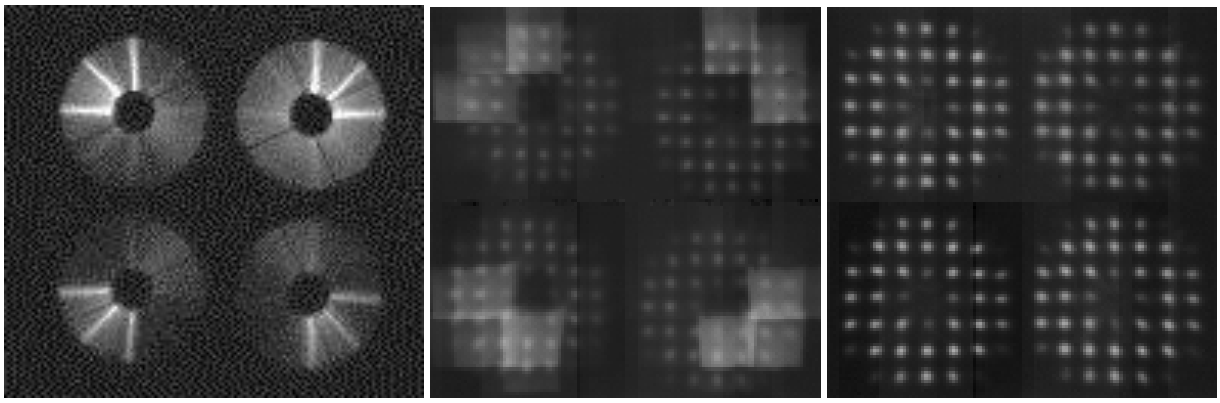

Figure 4 LGS pupil image (left), and raw mean pixel frames from LGS WFS showing Shack-Hartmann spot pattern from the laser launch system running at 10khZ (center) and 12kHz (right) for the 21km distant LGS with a 1.5km depth range gate.

3.3. Turbulence profiling

When operating in NGS-only mode, the projected pupils from each NGS WFS separate at a distance of 18-20km from the telescope pupil, dependant on the NGS asterism being observed. Due to the cone effect from the 21km distant LGS, the LGS pupils separate at approximately 10km. To fully characterise LGS tomographic performance it is therefore critical to have a good knowledge of the turbulence profile.

The CANARY NGS and LGS WFSs run in open-loop and can therefore be used to determine a profile whilst the system is applying correction to the DM. Data from these open-loop WFSs can either be used as a multiple set of SLODAR baselines, or analysed tomographically using data from all WFSs. However, this approach requires 2-3 minutes of observations before a profile can be measured. For an experimental system such as CANARY this overhead is acceptable and used routinely as part of the system calibration procedure.

However, when CANARY is operating without NGS, the LGS separation means that the altitude of the highest turbulent layers cannot be determined. We have recently developed a new dual camera SCIDAR instrument [21] that has been installed on the 1m Jacobus Kapteyn Telescope. This instrument not only provides very high vertical resolution profiles up to altitudes of ~18km (depending on binary star separation), but can also provide wind velocities for each detected layer. Whilst this information is not required to determine the Learn and Apply reconstructor, it can be used as an input for reconstructors such as the LQG control used in CANARY that can make use of temporal information. CANARY also makes use of a separate 0.5m SLODAR instrument situated on the roof of the WHT building to can probe the lowest 6-8km of the atmosphere with a vertical resolution of ~1km.

4. Results

4.1. Mixed NGS/LGS tomography

Due to availability of 4-star asterisms with stars $m_R<12$ during May in the northern hemisphere, the on-sky results presented here use a 3-star asterism (CANARY asterism 'T1') with only two off-axis NGS. Figure 5 shows the asterism used with the B-magnitudes of the central and two off-axis stars are 10.4, 11.0 and 11.1 respectively.

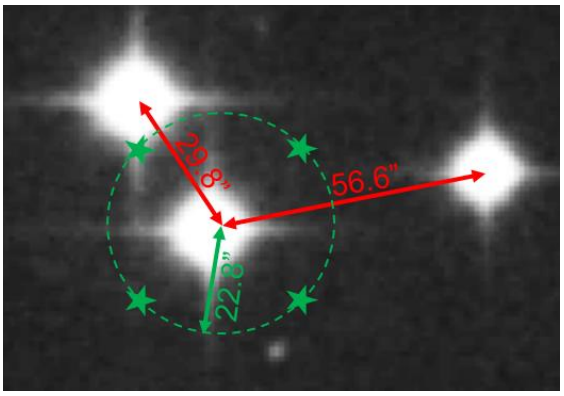

Figure 5 DSS image of CANARY Asterism T1 (α= 13 41 38.2 δ=+07 36 21 J2000) with the relative location of LGS asterism shown in green

The atmospheric profile (corrected for zenith angle) is shown in Figure 6. The observed profile showed a stronger fraction of turbulence strength at altitude than has typically been observed during the majority of CANARY observing nights, where a more standard profile would show 70-90% of the observed turbulence in the lowest altitude bin. A 3-layer tomographic reconstructor was calculated from this profile with correction being applied at altitudes of 0, 5 and 12km.

The plot in Figure 6 also shows measured CANARY on-sky performance for the system operating in SCAO, MOAO and GLAO (open-loop) configurations on asterism T1. Integration times for each data point were approximately 25s and all datasets were taken within an 11minute time frame. The performance that adding the tomographic information can achieve is best demonstrated through comparison between the GLAO and MOAO results. Adding tomographic information always improves performance, but it should be noted that the profile was particularly challenging for the CANARY tomographic LGS WFS system, where the correction of the high altitude layer at 12km was at the altitude limit of what can be achieved using the LGS. The variation in MOAO performance was thought to be due to high speed temporal variation of turbulence strength in the 12km layer, but this requires further analysis for confirmation.

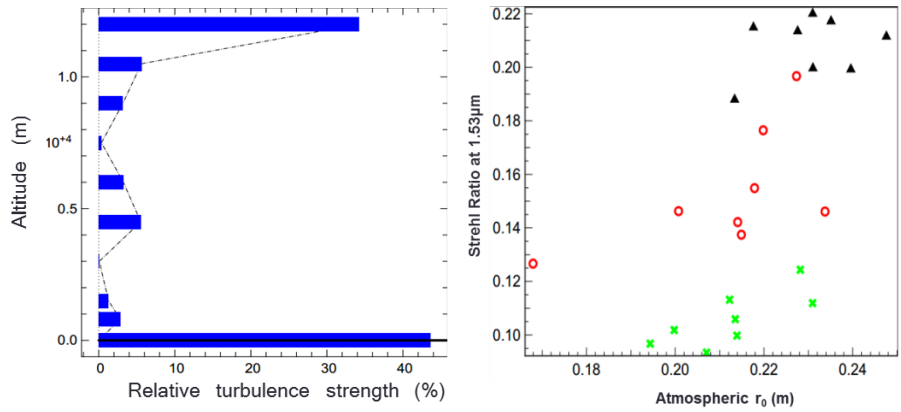

Figure 6 Relative turbulence strength versus altitude above the telescope in metres as observed by the CANARY open-loop NGS and LGS WFSs (left) and the effect of atmospheric turbulence strength (in terms of r_0 at 500nm) on 1530nm Strehl ratio for closed-loop SCAO correction (black triangles), and open-loop MOAO (red circles) and GLAO (green crosses)correction using all off-axis WFSs (right)

In addition to the use of all off-axis WFSs to perform open-loop tomographic correction, we also configured the system to use only tip and tilt signals from the off-axis NGS and utilise high-order information from the LGS WFSs only. The LGS asterism used in CANARY is near optimal for on-axis correction, allowing us to investigate Laser Tomographic AO (LTAO) performance in open-loop also. LTAO correction provided a Strehl ratio of 14.7%, comparable to the performance of MOAO, but further data analysis is required to fully characterise LGS-only tomographic performance.

4.2. Performance on emulated turbulence

The use of emulated turbulence contained within the CANARY telescope simulator allows a more comprehensive investigation of performance under a simplified, but static tomographic configuration. The telescope simulator was configured to emulate CANARY asterism 47 (α=18 27 08 δ=+26 52 34). CANARY performance under several possible tomographic configurations is shown in Figure 7. Turbulent layers within the simulator were conjugated to 0 and ~4.5km.

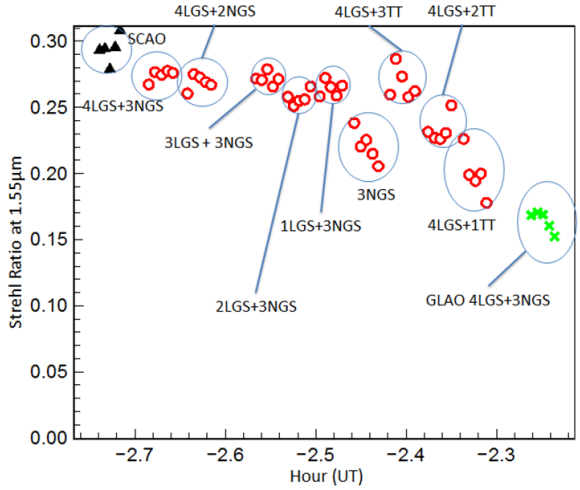

Figure 7 1550nm Strehl ratio for tomographic configurations possible (NGS high-order, LGS high-order and NGS used in tip-tilt (TT) only) from the 8 WFSs in CANARY.

Figure 7 shows that when the tomographic configuration (in terms of pupil sampling at the highest altitude layer), open-loop control and tomography can reliably achieve performance that is comparable to SCAO. Also, the use of LGS high-order signals with tip-tilt from off-axis NGS WFSs can result in performance that matches that of the 'full' mixed NGS/LGS tomography. This is an important result

that shows that the use of tomographic information from LGS can improve performance, and also that when the tomographic sampling is good, SCAO-like correction can be achieved.

4.3. Tomography using artificial neural networks

In this section we present the latest results from an on-going project to implement an Artificial Neural Network (ANN) as an open-loop Adaptive Optics tomographic reconstructor. For a full description of the concept see [22]. ANNs are computational models which consist of a series of interconnected simple processing elements called neurons, however the network needs to be trained before it can be used. During the training, the structure of the network is changed to adopt the structure of a determined function, based on a series of input-output data sets provided. Although each individual neuron implements its function imperfectly, the whole structure is capable of learning complex functions and solutions [23].

ANNs are trained by exposing them to a large number of inputs together with the desired output. Here we trained the ANN to reconstruct the open loop slopes predicted for the on-axis target, which were then converted into DM commands using the truth sensor control matrix. This resulted in a tomographic reconstructor with the benefit of stability even in dynamic atmospheric conditions.

We used the CANARY calibration bench to generate a training dataset and validated the corresponding neural network on the same bench. For the training the two available phase screens were placed as close together as possible. The screens were then counter rotated at different angular velocities to increase the variability of the phase that was measured. The phase screens were conjugated to the ground and then slowly moved up in conjugate altitude. 10000 frames of WFS slopes covering approximately 30s of emulated data were taken at each altitude step. The dataset thus includes the influence of turbulent layers at all possible altitudes.

To validate the ANN one of the phase screens was conjugated to the telescope pupil (as there is always a strong turbulent layer at the ground [24]) and the second over a range of higher conjugate altitudes. Figure 8 shows that the neural network does indeed behave as expected and maintained performance even with a changing turbulence profile. We then compared the ANN to Learn & Apply performance and found that *without re-learning* the performance of Learn and Apply drops below that of the ANN if the turbulence changes conjugate altitude by more than approximately 250 m.

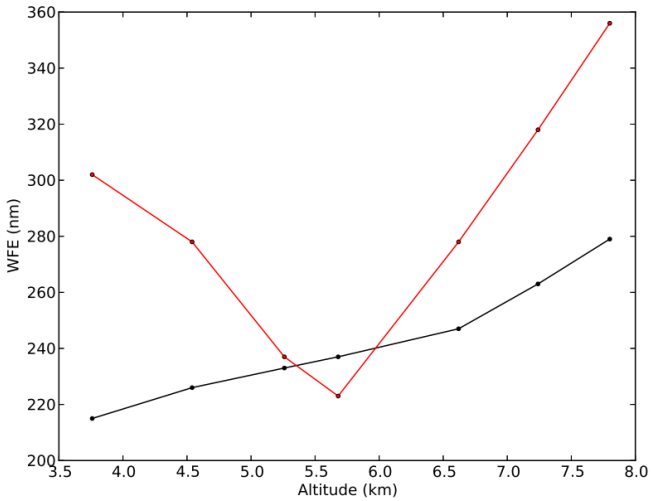

Figure 8 Residual WFE for L&A (red) and ANN (black) tomographic reconstructors on the CANARY calibration bench with the higher turbulent phase screen position at the given altitude

5. Conclusions

We have described the Phase B CANARY system and shown the on-sky and on-bench performance of the system under various NGS and LGS tomographic wavefront sensing configurations. We have presented initial results comparing SCAO with open-loop MOAO, GLAO and LTAO on-sky performance that prove the use of information on high-altitude turbulence derived from off-axis WFS data can be beneficial for AO correction, and at times approach that of SCAO systems. We have also demonstrated that an ANN tomographic reconstruction can be used on a real-world system and result in a reconstructor that is insensitive to changes in turbulence altitude.

The on-sky performance of MOAO falls between that of SCAO and GLAO, although MOAO performance can be variable in the presence of a strong high-altitude turbulent layer, particularly with the use of tomographic information derived from relatively low-altitude Rayleigh LGS. When the tomographic configuration is more favourable, with well-sampled layers at low altitude (as investigated using the telescope simulator) open-loop tomography matches SCAO performance. It should be noted that the 4.2m diameter of the WHT is at the lower limit for performing accurate tomography due to the altitude at which pupil separation occurs. Tomography on larger telescopes should show less variability with better sampling of higher altitude turbulent layers.

References

1. F. Hammer, M. Puech, F. Assemat *et al*, Proc. SPIE, **5382**, pp 727-736, (2004)
2. C. Baranec, M. Hart, N. M. Milton *et al*, ApJ, **693**, p1814, (2009)
3. E. Marchetti, N. Hubin, E. Fedrigo *et al*, Proc. SPIE, **4839**, pp 317-328, (2003)
4. F. Rigaut *et al*., Proc. SPIE, **8447**, p. 84470I, (2012)
5. R. Myers, Z. Hubert, T. Morris *et al.*, Proc. SPIE, **7015**, p. 70150E, (2008)
6. E. Marchetti *et al.*, *OSA Adaptive Optics: Methods, Analysis and Applications*, p. AMA2, (2007)
7. F. Vidal, B. Neichel, F. Rigaut *et al.*, *This conference*, p. 13276 (2013)
8. F. Rigaut, *ESO Conf. Beyond Convent. Adapt. Opt*., pp. 11-16, (2002)
9. M. Lloyd-Hart, C. Baranec, N. M. Milton *et al*, Opt. Express **14**, 17, pp. 7541-7551, (2006)
10. E. Gendron, F. Vidal, M. Brangier *et al*, A&A, **529**, L2, (2011)
11. D. Gavel *et al*, Proc. SPIE, **6888**, p688804, (2008)
12. D. Andersen *et al*, Proc. SPIE, **7015**, p70150H , (2008)
13. M. Ammons *et al*, Proc. SPIE, **6272**, p627202, (2006)
14. F. Assemat, E. Gendron and F.Hammer, MNRAS, **376**, p. 287-312, (2007)
15. J-G Cuby, S. Morris, I. Bryson *et al.*, Proc. SPIE, **7014**, p. 70141K, (2008)
16. D. Andersen *et al.*, in *Proceedings of AO4ELT2*, (2012)
17. A. Basden, D. Geng, R. Myers and E. Younger, Appl. Opt. **49**, pp. 6354-6363, (2010)
18. A. Basden and R. Myers, MNRAS, **424**, pp. 1483-1494, (2012)
19. F. Vidal, E.Gendron, G .Rousset, JOSA A, **27**, p. 253-264, (2012)
20. G. Sivo, C. Kulcsar, J-M Conan *et al.*, *This conference*, p. 13353, (2013)
21. J. Osborn, R. Wilson, H. Shepherd *et al.*, *This conference*, p. 13302, (2013)
22. J. Osborn, F. J. D. C. Juez, D. Guzman, *et al.*, Opt. Express, **20**, pp. 2420–2434, (2012)
23. D. L. Reilly and L. N. Cooper, *An introduction to neural and electronic networks*, eds. S. F. Zornetzer, J. L. Davis, C. Lau, and T. McKenna, Ch. 12, Academic Press, (1990)
24. J. Osborn, R. W. Wilson, T. Butterley, H. Shepherd, and M. Sarazin, MNRAS, **406**, 2, pp. 1405–1408, (2010)